

# THERMOMECHANICAL MODEL FOR COMPACTED BENTONITE

PETRI JUSSILA

Helsinki University of Technology  
Institute of Mathematics  
Box 1100, FIN-02015 HUT  
e-mail: Petri.Jussila@hut.fi

## ABSTRACT

A general thermomechanical model is derived for a mixture. The system is described by proper choices of free energy and dissipation function. The general theory is applied to a TH model for a bentonite buffer. The free energy of the system is chosen to take into account the individual behaviours of the components and their mutual interactions. The resulting thermodynamically consistent macroscopic model is fitted to a suction experiment and applied to a simple 1D TH simulation of the bentonite buffer of the Febex in situ test. The results calculated with FEM are compared to measurements.

## 1. INTRODUCTION

A buffer of compacted bentonite is planned to be used to prevent the movement of groundwater and the consequential escape of material from a geological repository for spent nuclear fuel. Fluid flow, phase changes, mechanical behaviour of the buffer, rock, and the waste canisters, and the heat produced by the waste constitute a coupled thermohydromechanical system. The aim of the study is to derive a general thermodynamically consistent THM model for an arbitrary mixture. The general theory is applied to the thermohydraulic modelling of a mixture of compacted bentonite, liquid water, vapour, and air.

The system is described by proper choices of free energy and dissipation function. The free energy of the system is chosen to take into account the individual behaviours of the components and their mutual interactions through adsorption, vaporisation, and mixing of the gaseous components. The choice is based on the equilibrium conditions for the water species in different combinations of the components.

The model is fitted to a suction experiment for Febex bentonite and applied to the TH simulation of the bentonite buffer of the Febex in situ test, which is considered in the international Decovalex 3 project. The present approach is to describe the essential features of the TH behaviour of the buffer in a simple 1D geometry. The results calculated with FEM are compared to the measurements.

## 2. THE GENERAL MODEL

The system consists of solid skeleton (s), liquid water (l), water vapour (v), and air (a). Vapour and air occupy the same gaseous (g) volume fraction. The molar volume fraction  $\xi_k = \beta_g x_k$  for  $k \in \{a, v\}$  and  $\xi_k = \beta_k x_k$  for  $k \in \{s, l\}$  of component  $k$  is defined by means of the volume fraction  $\beta_j = V_j/V$  of the phase  $j \in \{s, l, g\}$  and the molar fraction  $x_k = n_k/(n_a+n_v)$  for  $k \in \{a, v\}$  and  $x_k = 1$  for  $k \in \{s, l\}$  of component  $k$ , where  $n_k$  [mol] is the mole number of component  $k$ . Apparently, we have  $\sum_k \xi_k = 1$ . The molar volume fractions relate the apparent densities  $\rho_k = m_k/V$  [kg/m<sup>3</sup>] to the

intrinsic densities  $\tilde{\rho}_k = m_k/(x_k V_j)$  [kg/m<sup>3</sup>], for which  $j = g$  for  $k \in \{a, v\}$  and  $j = k$  for  $k \in \{s, l\}$  by the equation  $\rho_k = \xi_k \tilde{\rho}_k$ .

We also define porosity  $\eta = 1 - \xi_s$ , liquid saturation  $\chi = \xi_l / (1 - \xi_s)$ , and vapour fraction  $\zeta = \xi_v / (\xi_a + \xi_v)$  as alternative variables.

In the general model the state variables are chosen to be the molar volume fractions  $\xi_k$ , intrinsic densities  $\tilde{\rho}_k$ , and strains  $\boldsymbol{\varepsilon}_k$  [-] of the components, and the common temperature  $T$  [K]. The indicator function taking care of the restriction for the molar volume fractions is

$$I(\xi_s, \xi_l, \xi_v, \xi_a) = \begin{cases} 0, & (\xi_s, \xi_l, \xi_v, \xi_a) \in C, \\ +\infty, & \text{otherwise,} \end{cases} \quad (1)$$

where the feasible set is

$$C = \left\{ (\xi_s, \xi_l, \xi_v, \xi_a) \in \square^4 \mid \sum_k \xi_k = 1, \xi_k \geq 0, k \in \{s, l, v, a\} \right\} \quad (2)$$

The free energy [J/m<sup>3</sup>] of the system is

$$\psi = \sum_{k \in \{s, l, v, a\}} \rho_k \psi_k = \sum_{k \in \{s, l, v, a\}} \rho_k \tilde{\psi}_k + TI(\xi_s, \xi_l, \xi_v, \xi_a), \quad (3)$$

where  $\tilde{\psi}_k$  [J/kg] is the specific free energy of component  $k$  without the restriction (2). Dissipative behaviour of the system is characterised by the dissipative variables, which in the general work are chosen to be the rates of deformation  $\mathbf{D}_k$  [1/s], the heat fluxes  $\mathbf{q}_k$  [W/m<sup>2</sup>], and the relative velocities  $\mathbf{V}_k$  [m/s]. The dissipation function  $\phi$  [W/m<sup>3</sup>] is a function of the state variables and the dissipative variables.

We follow the procedure introduced in [1] of using the principle of maximal rate of entropy production [2] with the orthogonality relations

$$\phi = \nu \left[ \sum_k (\partial \phi / \partial \mathbf{D}'_k) : \mathbf{D}'_k + (\partial \phi / \partial (\text{tr} \mathbf{D}_k)) \text{tr} \mathbf{D}_k + (\partial \phi / \partial \mathbf{q}_k) \cdot \mathbf{q}_k + (\partial \phi / \partial \mathbf{V}_k) \cdot \mathbf{V}_k \right], \quad (4)$$

$$\nu = \phi \left[ \sum_k (\partial \phi / \partial \mathbf{D}'_k) : \mathbf{D}'_k + (\partial \phi / \partial (\text{tr} \mathbf{D}_k)) \text{tr} \mathbf{D}_k + (\partial \phi / \partial \mathbf{q}_k) \cdot \mathbf{q}_k + (\partial \phi / \partial \mathbf{V}_k) \cdot \mathbf{V}_k \right]^{-1}. \quad (5)$$

As a result we get the following general constitutive relations

$$\boldsymbol{\sigma}'_k = \rho_k \frac{\partial \tilde{\psi}_k}{\partial \boldsymbol{\varepsilon}'_k} + \nu \frac{\partial \phi}{\partial \mathbf{D}'_k}, \quad (6)$$

$$p_k = -\rho_k \frac{\partial \tilde{\psi}_k}{\partial (\text{tr} \boldsymbol{\varepsilon}_k)} - \nu \frac{\partial \phi}{\partial (\text{tr} \mathbf{D}_k)} + p_k^{\text{th}}, \quad (7)$$

$$s_k = -\frac{\partial \tilde{\psi}_k}{\partial T} - \frac{I}{\tilde{\rho}_k}, \quad (8)$$

$$-\frac{\nabla T}{T} = \nu \frac{\partial \phi}{\partial \mathbf{q}_k}, \quad (9)$$

$$-\mathbf{m}_k - \sum_j \left( \rho_k \frac{\partial \tilde{\psi}_k}{\partial \xi_j} + \xi_k B \right) \nabla \xi_j + \sum_j \left( \rho_j \frac{\partial \tilde{\psi}_j}{\partial \xi_k} + \xi_j B \right) \nabla \xi_k = \nu \frac{\partial \phi}{\partial \mathbf{V}_k}, \quad (10)$$

$$p_k^{\text{th}} = \xi_k \tilde{\rho}_k^2 \frac{\partial \tilde{\psi}_k}{\partial \tilde{\rho}_k} - \xi_k T I, \quad (11)$$

$$G_q - G_p = 0, \quad (12)$$

where  $\boldsymbol{\sigma}'_k$  [Pa] is the deviatoric Cauchy stress,  $p_k$  [Pa] is the pressure,

$$p_k^{\text{th}} = \xi_k \left( B + \sum_j \rho_j \frac{\partial \tilde{\psi}_j}{\partial \xi_k} \right) \quad (13)$$

is the relative thermodynamical pressure [Pa],  $B$  [Pa] is the relative hydrostatic pressure for which

$$B = \left\{ B_k \forall k \in \{s, l, v, a\} \mid (B_s, B_l, B_v, B_a) \in T \partial I(\xi_s, \xi_l, \xi_v, \xi_a) \right\}, \quad (14)$$

$s_k$  [J/(kgK)] is the specific entropy,  $\mathbf{m}_k$  [N/m<sup>3</sup>] is the rate of production of linear momentum, and

$$G_k = \tilde{\psi}_k - \frac{1}{2} \mathbf{U}_k \cdot \mathbf{U}_k + \frac{p_k^{\text{th}}}{\rho_k} \quad (15)$$

is the generalised specific Gibbs function [J/kg], where  $\mathbf{U}_k$  [m/s] is the absolute velocity of component  $k$ .

### 3. THERMOHYDRAULIC MODELLING OF BENTONITE

#### 3.1 Constitution

The general theory is applied to thermohydraulic modelling of bentonite buffer with an assumption of a rigid skeleton. We get the constitution from the general constitutive relations with appropriate choices of the free energies and the dissipation function. The chosen specific free energies of the components are the following

$$\psi_s(T, \tilde{\rho}_s, \xi_j) = -c_s T \ln \frac{T}{T_0} + \frac{T}{\tilde{\rho}_s} I(\xi_j), \quad (16)$$

$$\psi_l(T, \tilde{\rho}_l, \xi_j) = -c_l T \ln \frac{T}{T_0} + \frac{RT}{M_v} h(\xi_s, \xi_l) + \frac{T}{\tilde{\rho}_l} I(\xi_j), \quad (17)$$

$$\psi_v(T, \tilde{\rho}_v, \xi_j) = -c_v T \ln \frac{T}{T_0} + \frac{RT}{M_v} \ln \frac{\tilde{\rho}_v}{\tilde{\rho}_{v,0}} + \frac{RT_0}{M_v} \frac{\tilde{\rho}_{v,0}}{\tilde{\rho}_v} + f(T) + \frac{RT}{M_v} g_v(\xi_j) + \frac{T}{\tilde{\rho}_v} I(\xi_j), \quad (18)$$

$$\psi_a(T, \tilde{\rho}_a, \xi_j) = -c_a T \ln \frac{T}{T_0} + \frac{RT}{M_a} \ln \frac{\tilde{\rho}_a}{\tilde{\rho}_{a,0}} + \frac{RT_0}{M_a} \frac{\tilde{\rho}_{a,0}}{\tilde{\rho}_a} + \frac{RT}{M_a} g_a(\xi_j) + \frac{T}{\tilde{\rho}_a} I(\xi_j), \quad (19)$$

where  $c_k$  [J/(kgK)] is the specific heat at constant volume,  $M_k$  [kg/mol] is the molar weight,  $R$  [J/(mol K)] is the universal gas constant,  $f$  [J/kg] is a vaporisation function,  $h$  [-] is an adsorption function,  $g_k$  [-] is a mixing interaction term for the gaseous components, and  $\tilde{\rho}_{k,0}$  [kg/m<sup>3</sup>] is the intrinsic density at the reference state  $(P, T) = (P_0, T_0)$ , where  $P$  [Pa] is the (mixture) pressure.

The chosen forms for the adsorption function, mixing terms, and vaporisation function, respectively, are

$$h(\xi_s, \xi_l) = b \left( \frac{\xi_s}{\xi_l} - \frac{1}{\chi_{\max}} \frac{1 - \eta_0}{\eta_0} \right)^2 = a \left( \frac{1}{\chi} - \frac{1}{\chi_{\max}} \right)^2, \quad (20)$$

$$g_k(\xi_v, \xi_a) = \ln \left( \frac{\xi_k}{\xi_a + \xi_v} / \frac{\xi_{k,0}}{\xi_{a,0} + \xi_{v,0}} \right), \quad k \in \{a, v\}, \quad (21)$$

$$f(T) = -\frac{RT}{M_v} - L_0 \frac{T - T_0}{T_0}, \quad (22)$$

where  $\chi_{\max}$  [-] is the maximum saturation,  $a = b((1 - \eta_0) / \eta_0)^2$  is a constant material parameter, and  $L_0$  [J/kg] is a constant related to the latent heat of vaporisation.

The dissipation function is chosen to be

$$\begin{aligned} \phi(\mathbf{q}_j, \mathbf{V}_j, \mathbf{V}_{vg}) = & \sum_{k \in \{s, l, v, a\}} \left( \frac{1}{\xi_k \lambda_k T} \mathbf{q}_k \cdot \mathbf{q}_k \right) + \sum_{k \in \{l, g\}} \frac{\mu_k}{k_k} (\beta_k \mathbf{V}_k) \cdot (\beta_k \mathbf{V}_k) + \\ & + \tilde{\rho}_v \frac{RT}{M_v} \frac{1}{D} \frac{\beta_g}{\zeta(1 - \zeta)} (\zeta \mathbf{V}_{vg}) \cdot (\zeta \mathbf{V}_{vg}), \end{aligned} \quad (23)$$

where  $\lambda_k$  [W/(Km)] is the heat conductivity,  $\mu_k$  [kg/(sm)] is the dynamic viscosity,  $k_k$  [m<sup>2</sup>] is the permeability,  $D$  [m<sup>2</sup>/s] is the diffusivity,  $\mathbf{V}_g = \zeta \mathbf{V}_v + (1 - \zeta) \mathbf{V}_a$  is the molar weighted velocity of gas, and  $\mathbf{V}_{vg} = \mathbf{V}_v - \mathbf{V}_g$ .

The result for the relative intrinsic pressure denoted as  $\tilde{p}_k = p_k / \xi_k$  gets the form

$$\tilde{p}_k = B + \tilde{\rho}_l \frac{RT}{M_v} \xi_l \frac{\partial h}{\partial \xi_k}, \quad k \in \{s, l, v, a\}, \quad (24)$$

$$\tilde{p}_k = \tilde{\rho}_k \frac{RT}{M_k} - \tilde{\rho}_{k,0} \frac{RT_0}{M_k} - TI = P - P_0 - TI, \quad k \in \{v, a\}. \quad (25)$$

Here, the relative hydrostatic pressure  $B = P - P_0$  is found to equal to the mixture pressure.

The Darcy law for liquid, the Darcy law for gas, the Fick law for the relative velocity of vapour, and the Fourier heat conduction law, respectively, get the form

$$\beta_l \mathbf{V}_l = -\frac{k_l}{\mu_l} \left[ \nabla \left( \frac{p_l}{\xi_l} \right) - \tilde{\rho}_l \mathbf{g} + \tilde{\rho}_l \frac{RT}{M_v} \nabla h \right], \quad (26)$$

$$\beta_g \mathbf{V}_g = -\frac{k_g}{\mu_g} \left[ \nabla P - \frac{\rho_a + \rho_v}{\beta_g} \mathbf{g} \right], \quad (27)$$

$$\zeta \mathbf{V}_{vg} = -D \left[ \nabla \zeta - \zeta(1 - \zeta) \frac{M_v - M_a}{RT} \mathbf{g} \right], \quad (28)$$

$$\mathbf{q}_k = -\xi_k \lambda_k \nabla T. \quad (29)$$

Component interactions are studied by considering the Gibbs equilibrium (12) of the water species in different mixtures. The resulting Clausius-Clapeyron equations “outside” and “inside” the porous medium, respectively, are

$$\ln \frac{\zeta^0 P^0}{\zeta_0 P_0} = \frac{M_v}{RT} \left[ L_0 \frac{T-T_0}{T_0} + (c_v^p - c_l^p) T \ln \frac{T}{T_0} + \frac{P^0 - P_0}{\tilde{\rho}_1} \right], \quad (30)$$

$$\ln \frac{\zeta P}{\zeta_0 P_0} = \frac{M_v}{RT} \left[ L_0 \frac{T-T_0}{T_0} + (c_v^p - c_l^p) T \ln \frac{T}{T_0} + \frac{P - P_0}{\tilde{\rho}_1} \right] + h + \xi_1 \frac{\partial h}{\partial \xi_1}, \quad (31)$$

where  $\zeta P$ ,  $\zeta^0 P^0$ , and  $\zeta_0 P_0$  denote the partial pressure of saturated vapour from the gaseous phase inside the porous medium, outside the porous medium, and at the reference state, respectively. This is compatible with the conventional equilibrium conditions for ideal vapour with the assumptions  $c_l^p = c_l$ ,  $c_v^p = c_v + R/M_v$ , and  $L = L_0 + (c_v^p - c_l^p)T$ , where  $c_k^p$  [J/(kgK)] is the specific heat at constant pressure and  $L$  [J/kg] is the latent heat.

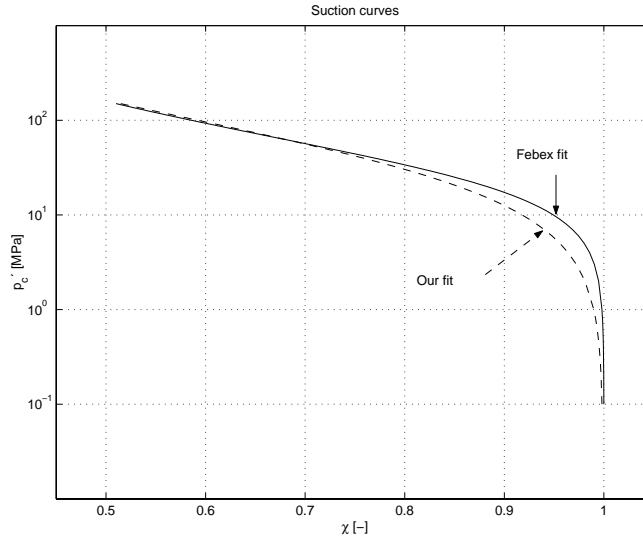


Figure 1. The suction curve (dashed) and the Febex fit (solid). The wetting experiment of a confined sample with  $\rho_{dry} = 1600 \dots 1650 \text{ kg/m}^3$ .

By combining the Gibbs equilibria (30, 31) at the same pressure and temperature we get the relative humidity inside the porous medium as

$$\ln RH = \ln \left( \frac{\zeta P}{\zeta^0 P^0} \right) = \ln \left( \frac{\zeta}{\zeta^0} \right) = h + \xi_1 \frac{\partial h}{\partial \xi_1} \quad (32)$$

and the Kelvin law for the suction pressure  $p_c$  by means of the adsorption function as

$$p_c = -\tilde{\rho}_1 \frac{RT_0}{M_v} \left( h + \xi_1 \frac{\partial h}{\partial \xi_1} \right), \quad (33)$$

which form is also presented in [3]. The fitted suction curve by means of (20, 33) along with a van Genuchten fit used in the Febex project is plotted in Figure 1.

### 3.2 The thermohydraulic model

The final state variables are saturation  $\chi$ , temperature  $T$ , and vapour fraction  $\zeta$ . Inertial terms and gravitation are neglected and the total pressure is assumed to be constant. The model consists of the conservation of the mass of the water species, and the thermal energy conservation, i.e.,

$$\frac{\partial}{\partial t}(\rho_l + \rho_v) + \nabla \cdot [\tilde{\rho}_l \xi_l \mathbf{V}_l + \tilde{\rho}_v \xi_v \mathbf{V}_v] = 0, \quad (34)$$

$$c \frac{\partial T}{\partial t} - L \left( \frac{\partial \rho_l}{\partial t} + \nabla \cdot (\rho_l \mathbf{V}_l) \right) + \nabla \cdot \mathbf{q} = 0, \quad (35)$$

where  $c = \sum_k \rho_k c_k$ . The constitutive relations are reduced to the Clausius-Clapeyron equation, vapour state equation, Darcy's law for liquid, the result of Fick's law for vapour, Fourier's law for heat flow, and to the latent heat of vaporisation, i.e., to

$$\ln \frac{\zeta}{\zeta_0} = \frac{M_v}{RT} \left[ L_0 \frac{T - T_0}{T_0} + (c_v^p - c_l^p) T \ln \frac{T}{T_0} \right] + h + \xi_l \frac{\partial h}{\partial \xi_l}, \quad (36)$$

$$P = \tilde{\rho}_v \frac{RT}{M_v}, \quad (37)$$

$$\xi_l \mathbf{V}_l = \frac{k_l}{\mu_l} \tilde{\rho}_l \frac{R}{M_v} \frac{2a}{\chi^3} [\chi(1 - \chi/\chi_{\max}) \nabla T - T \nabla \chi], \quad (38)$$

$$\xi_v \mathbf{V}_v = -\beta_g D \nabla \zeta, \quad (39)$$

$$\mathbf{q} = \sum_k \mathbf{q}_k = -\sum_k \xi_k \lambda_k \nabla T \equiv -\lambda \nabla T, \quad (40)$$

$$L(T) = L(T_0) + (c_v^p - c_l^p)(T - T_0) = L_0 + (c_v^p - c_l^p)T, \quad (41)$$

respectively. The relation between saturation and relative humidity is given by equations (20, 32).

## 4. THERMOHYDRAULIC SIMULATION OF THE FEBEX IN SITU TEST

The thermohydraulic aspects of the Febex in situ test (Figures 2 and 3) are simulated in 1D polar co-ordinate  $r \in [R_1, R_2] = [0.485, 1.14]$  m. The simulation covers the radial distributions of relative humidity and temperature for the sections E1 and E2 in the directions RD1, RD2, RD3, and RD4, and the evolutions of relative humidity and temperature in 3 points (E1H, E1C, and E1G) of the section E1. The initial saturation is  $\chi_{\text{init}} = 0.54$  corresponding to  $RH = 38\%$ , and initial temperature is that of the surrounding rock, i.e.,  $T_{\text{init}} = T_r = 285.15$  K. The simulated sequence between  $-180 \dots 1000$  d is divided in three periods. The moisture boundary conditions are no-flow at the heater and full saturation at the rock for every case.

1. Days between  $-180 \dots 0$  d correspond to the isothermal saturation period between the construction and the starting of the heaters.
2. Days between  $0 \dots 53$  d correspond to the heater adjustment period, which is approximated by a linear increase of the heater temperature to the final value assessed by the measurements for each case (Table 2). The temperature boundary condition at the rock is of the Robin type  $\mathbf{q} = H(T - T_r)$  with a calibrated value of the heat transfer coefficient  $H$  [W/(m<sup>2</sup>K)].
3. Days between  $53 \dots 1000$  d correspond to the period of controlled heating during which the temperature of the hottest point on each heater is kept at 373.15 K. The period is simulated

by keeping the heater temperature constant. The other boundary conditions are the same as for the period 2.

The results are calculated with the FEM program ELMER [4] in co-operation with CSC. The simple 1D mesh consists of 40 linear elements. A time step of 1 d is used for every case.

For heat capacity, heat conductivity, and liquid permeability, respectively, the following empirical relations are employed

$$c = c_{\text{eff}}(\chi, T) = \eta_0 \chi \bar{\rho}_1 c_1 + \rho_{\text{dry}} (1.38(T - 273.15) + 732.5), \quad (42)$$

$$\lambda = \lambda_{\text{eff}}(\chi) = A_2 + \frac{A_1 - A_2}{1 + e^{(\chi - x_0)/dx}}, \quad (43)$$

$$k_1 = k_1(\chi) = k_{\text{sat}} \chi^3, \quad (44)$$

where  $A_1$  and  $A_2$  [W/(Km)] are the thermal conductivities for dry and fully saturated medium, respectively,  $x_0$  [-] is the saturation for which the thermal conductivity is the average value between the extreme values,  $dx$  [-] is a parameter, and  $k_{\text{sat}}$  [ $\text{m}^2$ ] is the permeability of the fully saturated medium. For diffusivity of vapour-air mixture we use the relation  $D = D_1(T/T_1)^n$  [5]. The parameter values are given in Table 1.

The simulated and measured results for the evolution of relative humidity at the points E1H, E1C, and E1G are illustrated in Figure 4. Figure 5 shows the radial distributions of relative humidity and temperature for section E1 in both the directions RD3 and RD4. Figure 6 shows the radial distributions of relative humidity and temperature for section E2 in both the directions RD3 and RD4. Figure 7 shows the radial distributions of relative humidity and temperature for both the sections E1 and E2 in the direction RD2. Figure 8 shows the radial distributions of relative humidity and temperature for both the sections E1 and E2 in the direction RD1.

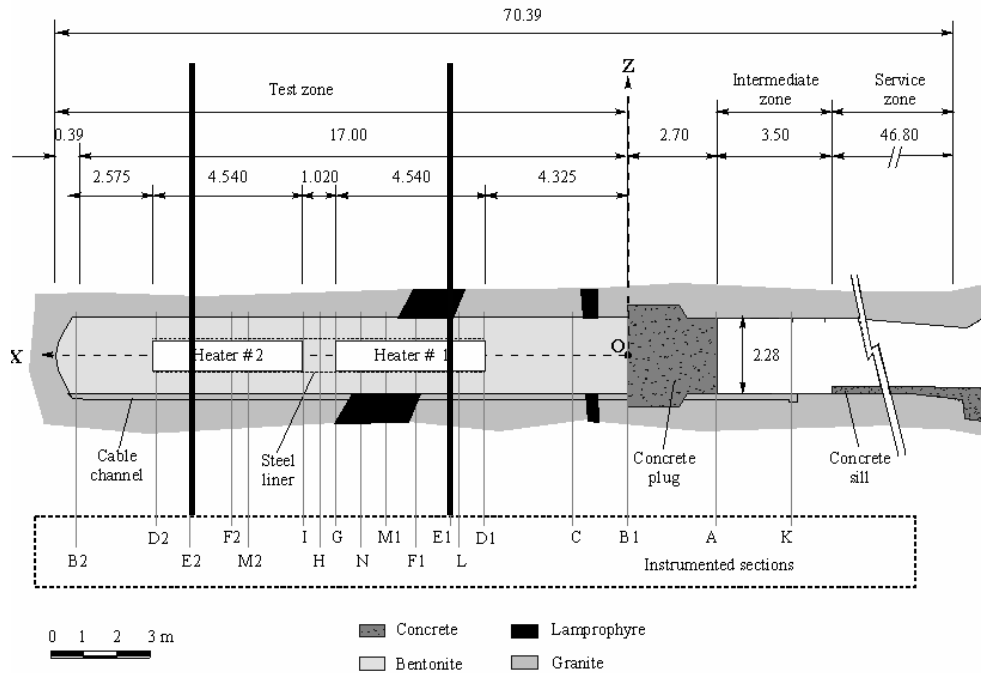


Figure 2. Profile of the Febex in situ experiment and the simulated sections E1 and E2.

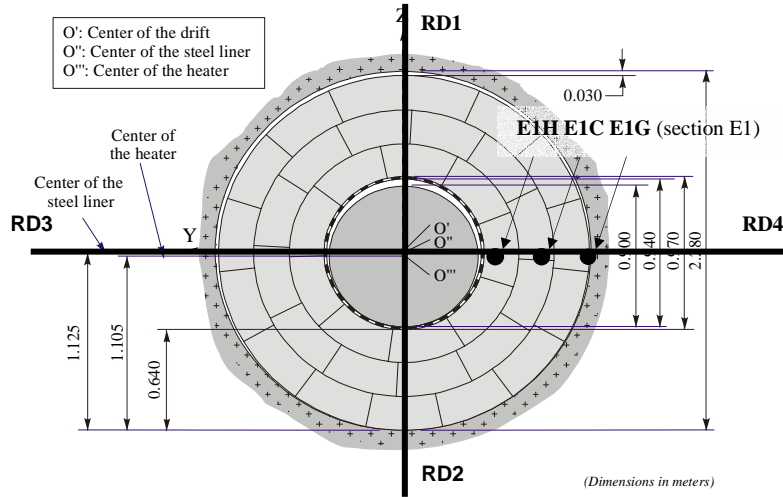


Figure 3. A typical Febex cross section with the definitions of the directions RD1, RD2, RD3, and RD4. The points E1H, E1C, and E1G of the section E1 correspond to  $r = 0.52$ ,  $0.81$ , and  $1.1$  m, respectively, in the 1D simulation.

Table 1. The parameters.

Initial and reference		Literature			Calibration		
Name	Value	Name	Value	Ref.	Name	Value	Case
$T_0$	293.15 K	$g$	$9.81 \text{ m/s}^2$		$a$	0.4	suction test
$P_0$	0.1013 MPa	$R$	$8.314 \text{ J/(mol K)}$		$H$	$1.9 \text{ W/(m}^2\text{K)}$	
$\eta_0$	0.45	$M_v$	$0.018 \text{ kg/(mol)}$		$T(R_1)$	266.15 K	E1;RD3, RD4
$\rho_{\text{dry}}$	$1690 \text{ kg/m}^3$	$\mu_l$	$1.0 \cdot 10^{-3} \text{ kg/(sm)}$	[6]	$T(R_1)$	269.15 K	E2;RD3, RD4
$\chi_{\text{max}}$	0.999	$\zeta_0$	0.023	[6]	$T(R_1)$	272.15 K	E1,E2; RD2
$\chi_{\text{init}}$	0.54	$D_1$	$0.216 \cdot 10^{-4} \text{ m}^2/\text{s}$	[5]	$T(R_1)$	253.15 K	E1,E2; RD1
$T_r$	285.15 K	$T_1$	273 K	[5]	<b>Laboratory test</b>		
		$n$	1.8	[5]	Name	Value	
		$c_v^p$	$1.87 \cdot 10^3 \text{ J/(kgK)}$	[6]	$A_1$	$0.57 \text{ W/(Km)}$	
		$c_l^p$	$4.18 \cdot 10^3 \text{ J/(kgK)}$	[6]	$A_2$	$1.28 \text{ W/(Km)}$	
		$L(T_0)$	$2.45 \cdot 10^6 \text{ J/kg}$	[6]	$x_0$	0.65	
		$\tilde{\rho}$	$998 \text{ kg/m}^3$	[6]	$dx$	0.10	
					$k_{\text{sat}}$	$2.0 \cdot 10^{-21} \text{ m}^2$	

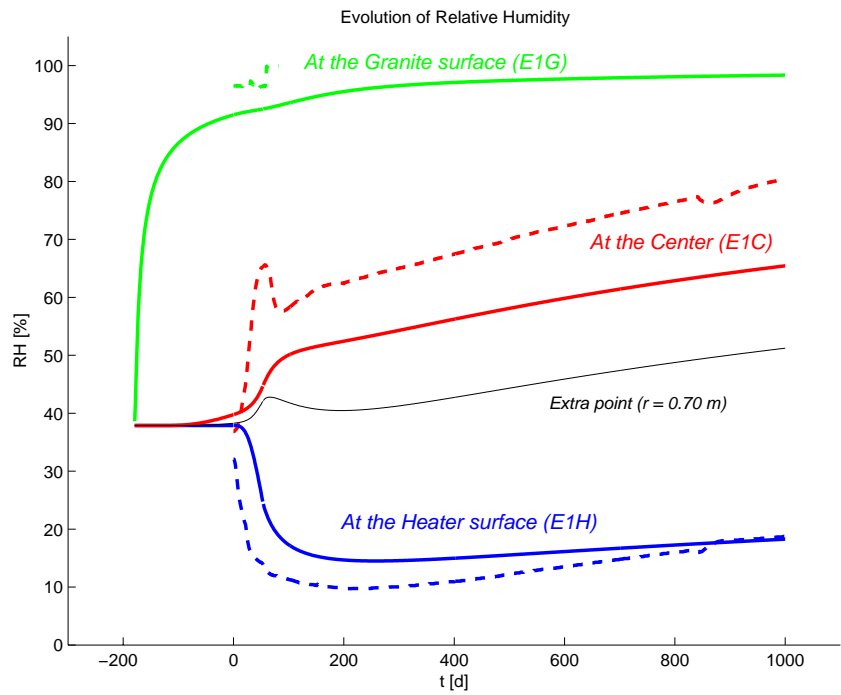


Figure 4. Simulated (solid) and measured (dash) evolution of relative humidity at the points E1H, E1C, and E1G. The thin solid curve shows the simulated extra point.

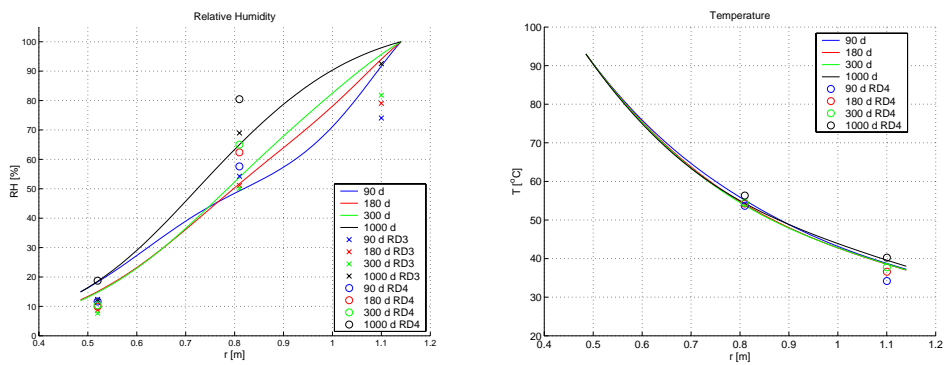


Figure 5. Simulated (curves) and measured (symbols) radial distributions of relative humidity (left) and temperature (right) at 90, 180, 300, and 1000 d for the section E1 in the directions RD3 and RD4.

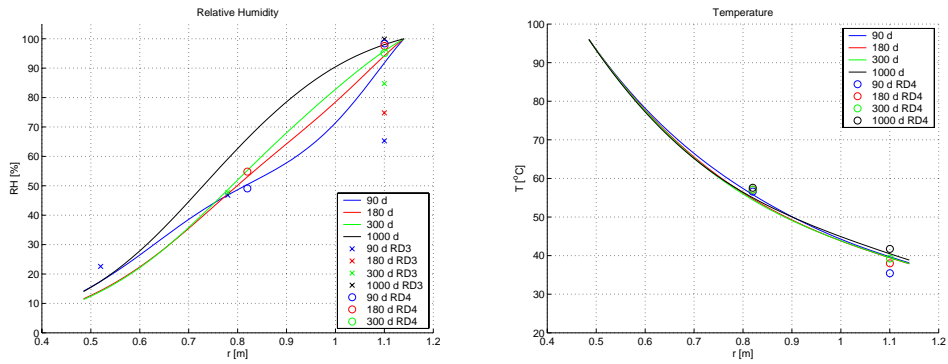


Figure 6. Simulated (curves) and measured (symbols) radial distributions of relative humidity (left) and temperature (right) at 90, 180, 300, and 1000 d for the section E2 in the directions RD3 and RD4.

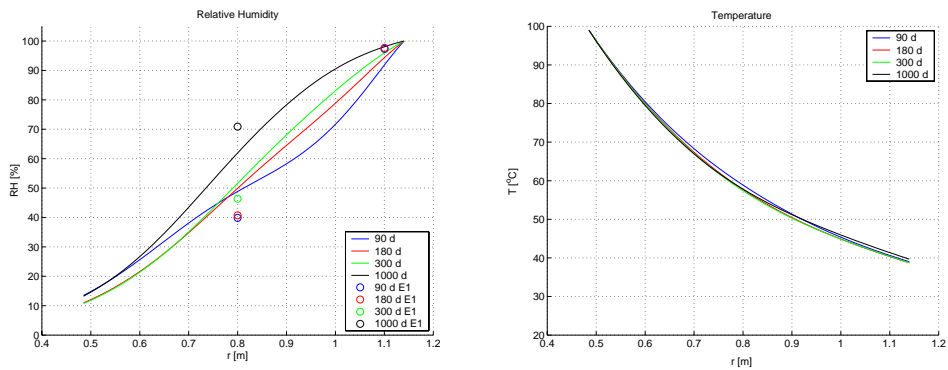


Figure 7. Simulated (curves) and measured (symbols) radial distributions of relative humidity (left) and temperature (right) at 90, 180, 300, and 1000 d for the sections E1 and E2 in the direction RD2.

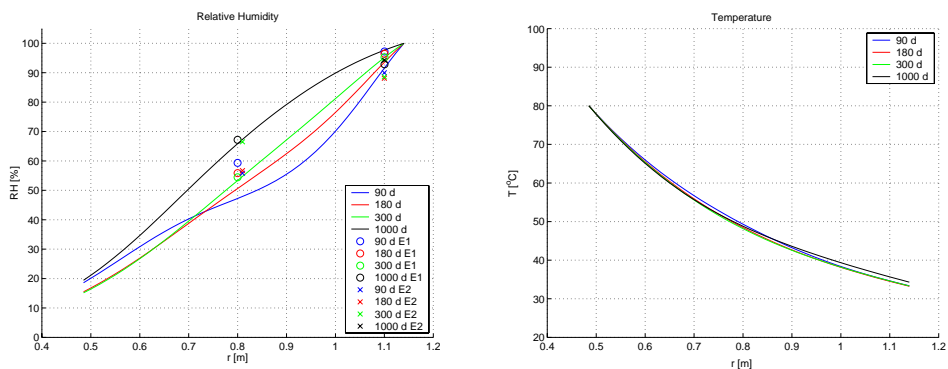


Figure 8. Simulated (curves) and measured (symbols) radial distributions of relative humidity (left) and temperature (right) at 90, 180, 300, and 1000 d for the sections E1 and E2 in the direction RD1.

## 5. CONCLUSIONS

The presented TH simulations are essentially simplified 1D predictions of the relative humidity by means of calibration of the temperature boundary conditions. The actual geometry, behaviours of the heater, liner and rock, and the deformation of the buffer are not considered. Convection heat transfer, pressure variation due to vaporisation, dependence of dynamic viscosity of liquid on temperature, and dependence of liquid density on temperature and pressure are neglected, and the gas diffusion is of a simple form. The main simulational simplifications are the approximation of the heater adjustment period by a linear time dependence of temperature, and the use of a full saturation boundary condition at the rock surface.

Because the heater performance is simulated by means of temperature boundary conditions, the lack of temperature data constitutes a source of uncertainty. Other main uncertainties are related to the initial moisture distribution in the buffer and to the effect of the construction gaps and the instrumentation.

Fitting of the model against the suction experiment is done only by means of a single wetting curve with shortage of data at the dry region.

The largest discrepancy between the measured and simulated results can be seen in the case of relative humidity evolution at the centre of the buffer after the starting of the heaters. First a rapid condensation is measured followed by a rapid vaporisation after a sufficient temperature increase. In the simulation the same effect of consecutive wetting and drying is seen in considerably less extent at the region nearer the heater, e.g., at the extra point depicted in Figure 4. We suggest that this discrepancy be due to the gaps and instrumentation present in the actual case.

Despite the simplifications and uncertainties the simulations and the observations are fairly consistent. The model succeeds in its aim to describe the essential features of the TH behaviour, i.e., heat transfer, vaporisation, fluid flow, gas diffusion, and suction induced by adsorption.

## 6. REFERENCES

- [1] Hartikainen, J., and Mikkola, M., *Thermomechanical model of freezing soil by use of the theory of mixtures*, In Proceedings of the 6th Finnish Mechanics Days, Aalto, J., and Salmi, T., (eds), 1997, 1–26.
- [2] Ziegler, H., Wehrli, C., *The derivation of constitutive relations from the free energy and dissipation function*, In *Advances in Applied Mechanics*, volume 25, pages 183-238, New York, 1988.
- [3] Frémond, M., and Nicolas, P., *Macroscopic thermodynamics of porous media*, *Continuum Mechanics and Thermodynamics* 1990, 2:119-139.
- [4] CSC - The Finnish IT Center for Science, 21<sup>st</sup> January 2003, *ELMER*, [WWW document] <http://www.csc.fi/Elmer/>.
- [5] Vargaftik, N. B., *Tables on the thermophysical properties of liquids and gases. 2. ed.*, Wiley, New York, 1975.
- [6] Schmidt, E., *Properties of Water and Steam in SI-Units*, Springer, Berlin, 1989.